Annales Geophysicae (2004) 22: 1773–1786
SRef-ID: 1432-0576/ag/2004-22-1773
© European Geosciences Union 2004

Annales Geophysicae

On the propagation of bubbles in the geomagnetic tail

J. Birn[1], **J. Raeder**[2,5], **Y. L. Wang**[1,2], **R. A. Wolf**[3], **and M. Hesse**[4]

[1]Los Alamos National Laboratory, Los Alamos, New Mexico, USA
[2]University of California, Los Angeles, USA
[3]Rice University, Houston, Texas, USA
[4]NASA Goddard Space Flight Center, Greenbelt, Maryland, USA
[5]University of New Hampshire, Durham, New Hampshire, USA

Received: 20 August 2003 – Revised: 19 December 2003 – Accepted: 29 January 2004 – Published: 8 April 2004

Abstract. Using three-dimensional magnetohydrodynamic simulations, we investigate the propagation of low-entropy magnetic flux tubes ("bubbles") in the magnetotail. Our simulations address fundamental properties of the propagation and dynamics of such flux tubes rather than the actual formation process. We find that the early evolution, after a sudden reduction of pressure and entropy on a localized flux tube, is governed by re-establishing the balance of the total pressure in the dawn-dusk and north-south directions through compression on a time scale less than about 20 s for the typical magnetotail. The compression returns the equatorial pressure to its original unperturbed value, due to the fact that the magnetic field contributes only little to the total pressure, while farther away from the equatorial plane the magnetic field compression dominates. As a consequence the pressure is no longer constant along a flux tube. The subsequent evolution is characterized by earthward propagation at speeds of the order of 200–400 km/s, depending on the initial amount of depletion and the cross-tail extent of a bubble. Simple acceleration without depletion does not lead to significant earthward propagation. It hence seems that both the entropy reduction and the plasma acceleration play an important role in the generation of fast plasma flows and their propagation into the near tail. Earthward moving bubbles are found to be associated with field-aligned current systems, directed earthward on the dawnward edge and tailward on the duskward edge. This is consistent with current systems attributed to observed bursty bulk flows and their auroral effects.

Key words. Magnetospheric physics (magnetospheric configuration and dynamics; magnetotail; plasma sheet)

1 Introduction

The transport of plasma through the magnetosphere, and specifically the magnetotail, governs magnetospheric structure as well as its dynamics. It is generally recognized that, on average, there is a transport from the dayside to the nightside at high latitudes, and from higher latitudes on the nightside to lower latitudes. However, steady-state models of such transport or convection for realistic tail configurations are shown to be inconsistent with the combined conditions of frozen-in magnetic flux, and mass and entropy conservation (Erickson and Wolf, 1980; Schindler and Birn, 1982). Thus, it appears that the depletion of closed magnetic flux tubes by some process(es) plays a crucial role in permitting their transport from higher to lower latitudes or from the distant to the closer tail. In addition, Pontius and Wolf (1990) suggested that the depletion of a flux tube in itself might also be an important factor in the earthward acceleration in the form of a buoyancy force. Chen and Wolf (1993, 1999) supported this prediction through more quantitative approaches. Consistent with a lack of significant steady transport, observations also show that the plasma flow speed in the magnetotail is highly variable, with brief periods of fast plasma flow (bursty bulk flows) providing much of the sunward transport of mass, energy, and magnetic flux (e.g. Baumjohann et al., 1990; Angelopoulos et al., 1992). While BBFs may have features that appear to be inconsistent with the bubble model of Chen and Wolf, Sergeev et al. (1996b) reported observations of high-speed plasma flow bursts with properties consistent with this model.

Here we should inject a more precise definition of depletion, which is usually expressed as a reduction of the quantity pV^{γ}. This quantity is a measure of entropy per unit magnetic flux of a thin flux tube, where p is the plasma pressure, assumed to be constant along a field line or thin flux tube, and V is the flux tube volume per unit magnetic flux, defined by

Correspondence to: J. Birn
(jbirn@lanl.gov)

$$V = \int \frac{ds}{B} \tag{1}$$

integrated along a field line. Obviously, this definition is applicable only in relatively slowly evolving fields governed by instantaneous equilibrium (or at the beginning and the end of a sequence that leads from one equilibrium to another). In more general cases, when the plasma pressure is not constant along a field line, we replace the measure pV^γ with the integral

$$S = \int p^{1/\gamma} dV = \int p^{1/\gamma} \frac{ds}{B} \tag{2}$$

which becomes identical to

$$S = p^{1/\gamma} V \tag{3}$$

in case of equilibrium. We note that Eqs. (2) or (3) are based only on the pressure and the magnetic field, but not on density or temperature. Thus, a depleted flux tube may be of high or low temperature or density, and the entropy density (per unit mass), as measured by $p^{1/\gamma}/\rho$ may be reduced, enhanced or unchanged. Furthermore, the flux tube volume Eq. (1) or the entropy measure Eq. (2) are global properties that cannot directly be obtained from a local measurement. Hence, it is not clear whether flux tubes that are locally heated or compressed are inconsistent with a depletion.

Simulations of magnetic reconnection in the magnetotail (e.g. Birn et al., 1996b) have demonstrated that reconnection is indeed a powerful mechanism to reduce the volume, and hence the plasma and entropy content, of a reconnected flux tube, as well as to accelerate the plasma to fast speeds. However, the fact that reconnection causes both effects does not permit one to isolate the effects of buoyancy on a depleted flux tube. The present paper tries to investigate these effects by numerical integration of the acceleration and motion of depleted flux tubes in the magnetotail, deliberately excluding the actual formation process. Our scope is similar to that of Chen and Wolf (1999), but our approach differs in several aspects. First, we use a fully three-dimensional MHD code. Second, we also fully investigate the initial phase after the depletion, which was bypassed by Chen and Wolf by assuming that pressure equilibrium in y and z was re-established, while the pressure remained constant along the depleted field line.

By comparing the evolution of a depleted flux tube with one that also receives an initial impulse toward the Earth and one that receives an impulse but without depletion, we will also try to distinguish the effects of an initial impulse from that of the later acceleration. We further consider the effects of anisotropy through a double-adiabatic approach and investigate the role of the cross-tail width of the depleted flux tube and the mechanism of generation of field-aligned currents.

2 Initial states and numerical model

The initial magnetic field configuration is a self-consistent two-dimensional equilibrium, identical to the one used by Chen and Wolf (1999), given in dimensionless form by the vector potential

$$A = -\frac{1}{\alpha} \sin[\alpha(|z| - 1)] \exp(\alpha x) \qquad \text{for } |z| > 1 \tag{4}$$

$$A = \frac{2}{\pi} \cos\left(\frac{\pi}{2} z\right) \exp(\alpha x) \qquad \text{for } |z| \le 1 \tag{5}$$

with the corresponding unperturbed plasma pressure given by

$$p = p_0 \qquad \text{for } |z| > 1 \tag{6}$$

$$p = p_0 + \frac{A^2}{2}\left[\left(\frac{\pi}{2}\right)^2 - \alpha^2\right] \qquad \text{for } |z| \le 1, \tag{7}$$

where α=0.0816. We assume uniform temperature for the unperturbed initial state, so that the density is simply proportional to the pressure. We note that there is a difference in signs from the formulas given by Chen and Wolf (1999), because we use a coordinate frame with x being negative downtail, y pointing duskward and z northward, as in standard magnetospheric coordinates. The normalization units are the plasma sheet or current sheet half-width L (taken as 4 R_E by Chen and Wolf), the magnetic field strength for z=1 at the earthward boundary of the simulation box (B_L, equivalent to 37.5 nT in Chen and Wolf's units). The pressure unit is then given by B_L^2/μ_0. We also include a uniform background pressure p_0=0.025 to keep the Alfvén speed finite in the lobe regions $|z|>1$. As an additional third normalization unit we take a characteristic Alfvén speed of 1000 km/s. This choice implies an energy unit or temperature of ~5 keV, consistent with Chen and Wolf's choice, and a time unit of ~25 s.

The initial perturbation consists of a pressure (and temperature) reduction on a flux tube defined by unperturbed pressure values $0.15<p<0.175$ to approximately p=0.05. The equatorial crossing points of this depleted flux tube are initally located between $x=-7.4$ and $x=-8.5$. We considered three different widths of the depleted flux tube $|y|<y_m$ with y_m=0.02, 0.2, 2.0. Accordingly, we varied the width of the simulation box $0\le y\le y_{max}$, with y_{max}=0.2, 2.0, 10.0, respectively. The box size in x and z is given by $0\ge x\ge -10$ and $0\le z\le 2$, using symmetry at y=0 and z=0. As to be discussed later, in some of the runs we also imposed an initial earthward flow speed on the perturbed flux tube, to investigate the effect of an initial impulse versus subsequent acceleration. The evolution of the configuration was obtained by solving the dynamic MHD equations numerically, using an explicit finite-difference scheme (Birn et al., 1996a).

All boundaries of the simulation box, except for the symmetry boundaries and the distant tailward boundary $x=-10$, were treated as solid conducting boundaries. The distant boundary was treated as open to outflow, but no inflow was permitted. For some runs we doubled the box size in z and found that the location of the boundary in z has only negligible influence on the evolution. The effective field line tying at the near-Earth boundary might be expected to have a more

significant effect. From the results of Chen and Wolf (1999), however, we expect that these effects alter primarily the late evolution, when the depleted flux tubes approach the Earth.

3 Early evolution

The early evolution after the depletion of a flux tube is characterized by the re-establishment of the pressure balance in y and z. This is demonstrated by Figs. 1–4. Figure 1 shows the early evolution of a depleted flux tube, given by the pressure at the equatorial crossing point $x=-7.4$, $z=0$ as a function of y, for the three different flux tube widths. The figure demonstrates that pressure balance is re-established fast, although the time scales differ for the three cases, ranging from about 0.06 for $y_m=0.02$, to 0.35 for $y_m=0.2$, and 0.5 for $y_m=2.0$. The differences stem from the fact that the pressure increase for the wider flux tubes results mainly from a compression in z, while the narrowest flux tube becomes predominantly compressed in y. As a result this flux tube shows the most significant increase in B_z, demonstrated in Fig. 2. At the times when the pressure balance is re-established, B_z has increased by a factor of $\sim$2 for $y_m=0.02$, $\sim$1.3 for $y_m=0.2$, and $\sim$1.1 for $y_m=2.0$. We note that the increase of B_z at later times ($t>1$) in the top panel of Fig. 2 is not the result of the early compression but arises when the flow speed in x increases and the moving bubble plows through the plasma and field earthward of it, as discussed in the following section.

The evolution closer to Earth, away from the equatorial plane, is shown in Figs. 3 and 4 for p and B_x, respectively, at $x=-5.7$, $y=0$ as functions of z. Here the original pressure is not re-established. This is due to the fact that the contribution of B_x to the total pressure is more significant, so that a more modest compression can re-establish the balance of the total pressure. It is noteworthy that the increase of B_x from this compression (Fig. 4) implies a significant increase of the cross-tail current density on the inner edge of the depleted flux tube and a reversed current on the outer edge.

Figures 3 and 4 also demonstrate that the time scales for the three cases are much closer to each other at locations away from the equatorial plane. This results from the fact that the thickness of the depleted flux tube in z is significantly smaller at these locations, so that a compression takes a much shorter time. The cases for $y_m=0.2$ and $y_m=2.0$ (two top panels of Figs. 3 and 4) are basically undistinguishable. This is due to the fact that the compression is almost entirely in the z direction and hence essentially identical for the two cases.

In summary, the early evolution is governed by re-establishing the balance of the total pressure in y and z through compression on a time scale less than an Alfvén time. Only for very narrow flux tubes is this compression predominantly in y. The compression returns the equatorial pressure to its original unperturbed value, due to the fact that the magnetic field contributes only little to the total pressure, while at larger $|z|$ values the opposite is the case. As a consequence the pressure is no longer constant along a flux tube.

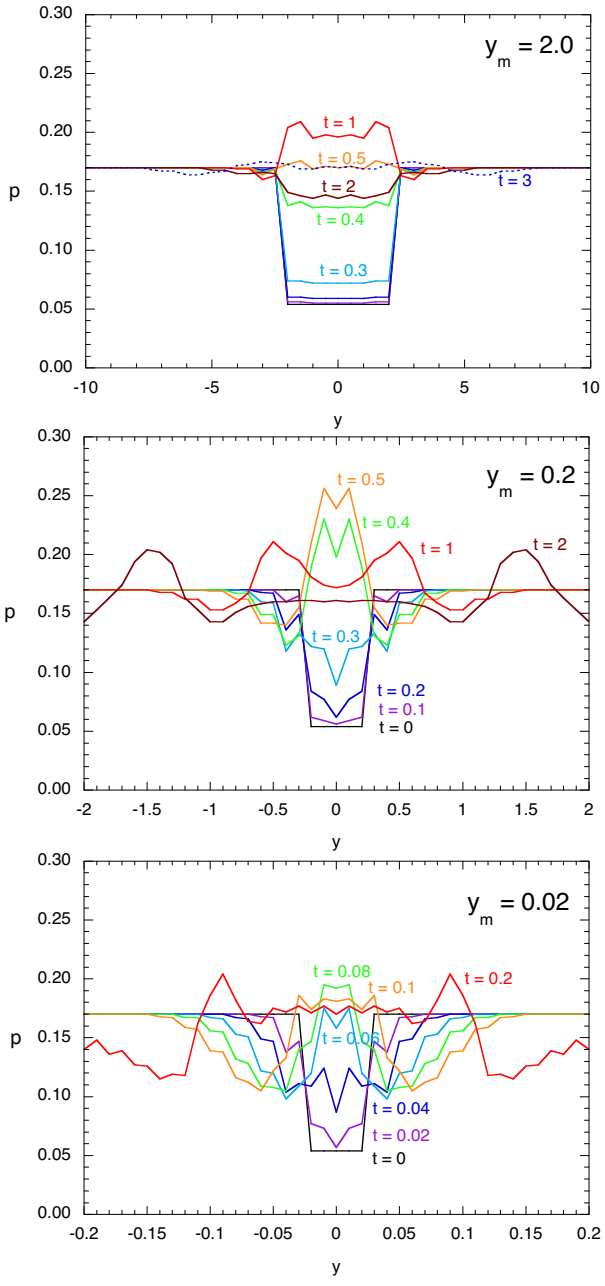

Fig. 1. Plasma pressure at $x=-7.4$, $z=0$ as a function of y at different times and for 3 different bubble widths, as indicated.

The re-establishment of this balance takes a much longer time. It is governed by the propagation of a compressional wave (that is, sound wave) along the flux tube and competes with the dynamic evolution of the flux tube. In the present simulations, we did not find that the pressure balance along the depleted flux tube was fully re-established during a typical run of 20-30 Alfvén times.

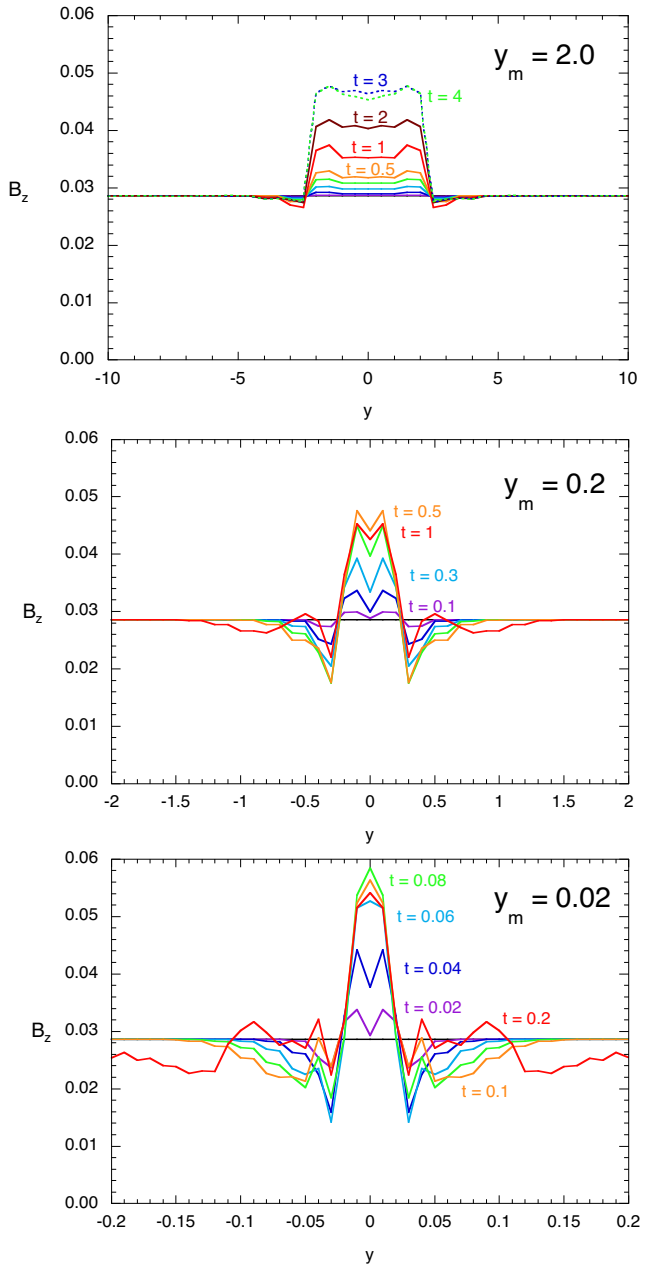

Fig. 2. Magnetic field B_z at x=−7.4, z=0 as a function of y at different times and for 3 different bubble widths, as indicated.

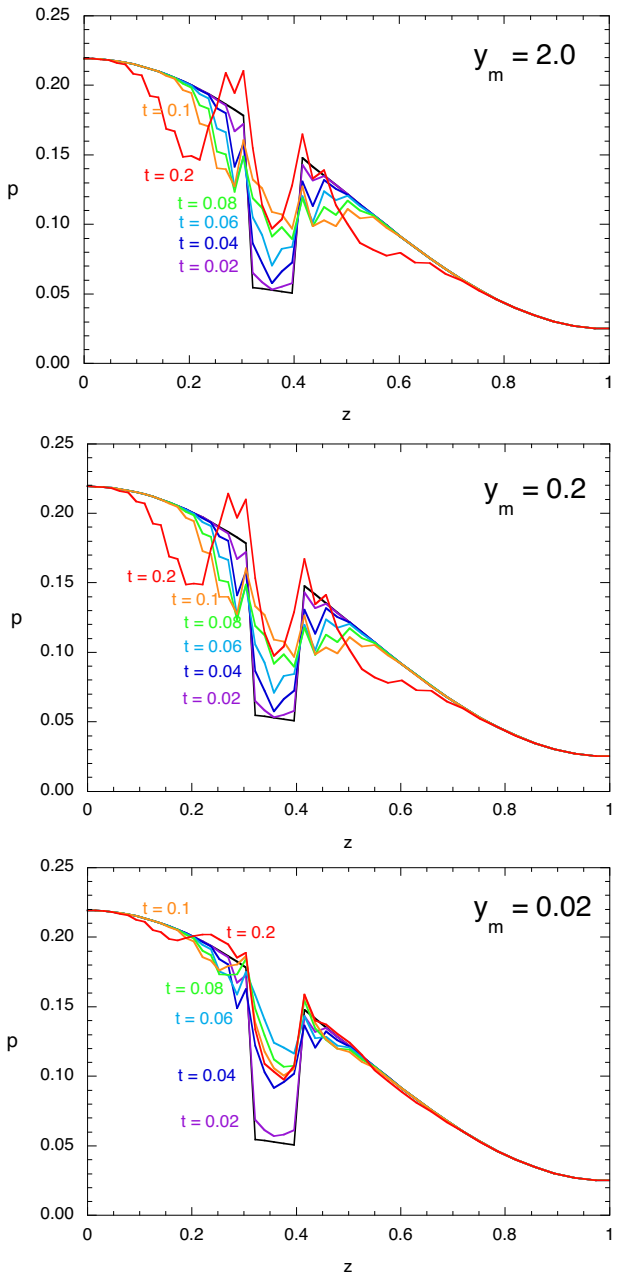

Fig. 3. Plasma pressure at x=−5.7, y=0 as a function of z at different times and for 3 different bubble widths, as indicated.

4 Later evolution

In Sect. 3, the early evolution for the first Alfvén period (approximately 25 s) was described. An overview of the subsequent evolution of a depleted flux tube is given in Fig. 5 for the intermediate size bubble with y_m=0.2. The color coding shows the velocity v_x in the midnight meridianal plane y=0. The solid lines are magnetic field lines that outline the extent of the depleted flux tube. These field lines are defined by the initial reduction of the entropy function $s=p^{1/\gamma}/\rho$. In an adiabatic transport model, this quantity should be conserved in a convected plasma element. Here we have calculated these field lines from the convection of the equatorial crossing point along z=0 by integration along the vector magnetic field at each instant of time. We can see that the bubble attains earthward speeds of ∼0.3, which spread from the vicinity of the equatorial plane along the flux tube earthward. The enhanced earthward flow remains well confined to the bubble. At later times, however, tailward flow develops on the outside of the bubble, which increases in speed as the earthward flow becomes reduced. This flow fills the void left behind by the earthward moving bubble.

The field-aligned earthward flow in the "horns" of the bubble reaches the near-Earth boundary at t≈15. The slow-down

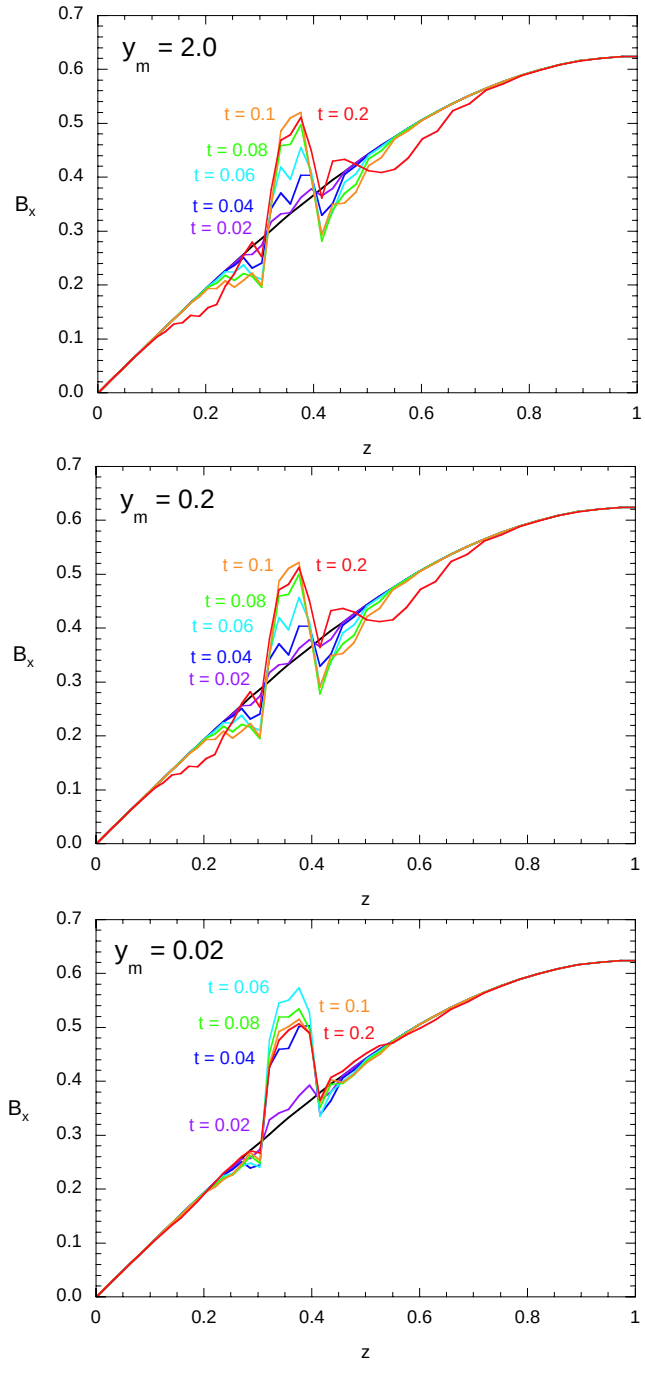

Fig. 4. Magnetic field B_x at x=−5.7, y=0 as a function of z at different times and for 3 different bubble widths, as indicated.

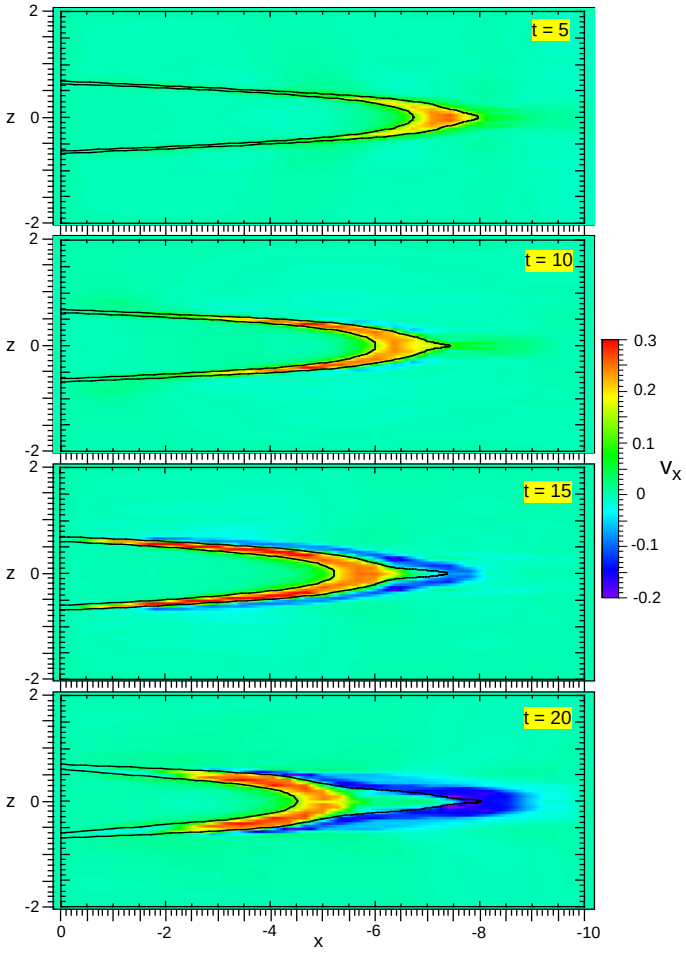

Fig. 5. Plasma velocity in the plane y=0 for y_m=0.2 at different times as indicated. The solid lines are magnetic field lines bounding the depleted flux tube.

then leads to a compression along the field direction and heating of the plasma in the near-Earth portions of the flux tube. As demonstrated by Fig. 6, the pressure then increases above the surrounding pressure and, to satisfy the pressure balance, the magnetic field decreases within the bubble due to an expansion in y and z. The localized reduction of the magnetic field corresponds to strong currents, which are opposite to the ones resulting from the initial perturbation: dawnward on the inner edge of the bubble and increased duskward current on the outer edge. These currents form extended layers in x, as shown in Fig. 7. They close around the bubble through northward and southward currents.

The evolution of pressure and velocity inside the bubble is shown in Fig. 8 for the depleted flux tube with y_m=0.2. The top panel shows the pressure and the second panel shows the velocity component v_x, which is mostly aligned with the magnetic field, except close to the equatorial plane. As demonstrated earlier, the early equilibration of the pressure balance leads to a stronger increase near the equatorial plane. The resulting pressure gradient along the field line leads to an acceleration of field-aligned flow towards the Earth. This flow is slowed down closer to Earth, leading to a pressure buildup, which eventually (after t∼15) reverses the pressure gradient and stops the earthward flow. In the final stage the pressure becomes approximately constant along the flux tube, which now has moved much closer to the Earth.

The evolution after the early equilibration is shown further in Fig. 9 for the narrow depleted flux tube (y_m=0.02). The top panel shows the propagation of a field line at the inner edge of the flux tube. The second panel shows the

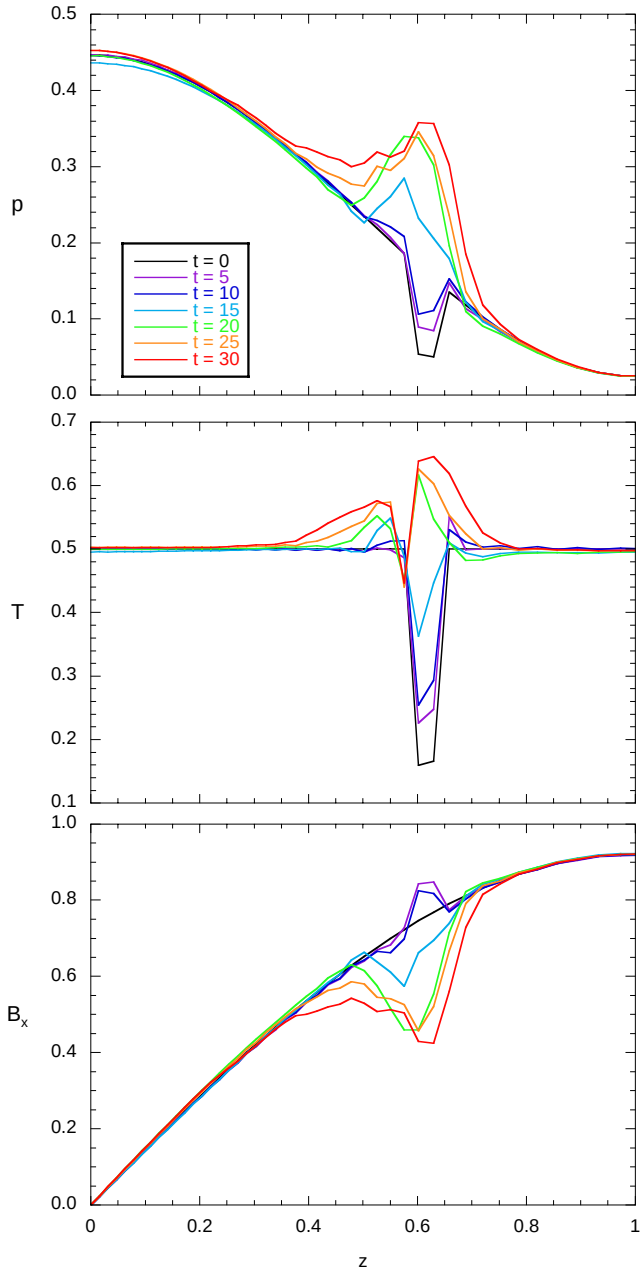

Fig. 6. Evolution of the near-Earth part of the depleted flux tube of Fig. 5, showing (from top to bottom) the plasma pressure, temperature, and the magnetic field component B_x with y_m=0.2 at x=−1.0, y=0 as functions of z for different times, as indicated by the color coding. Note that the initial pressure and temperature reduction and magnetic field enhancement become reversed as the flux tube fills through earthward flow and expands in the y and z directions.

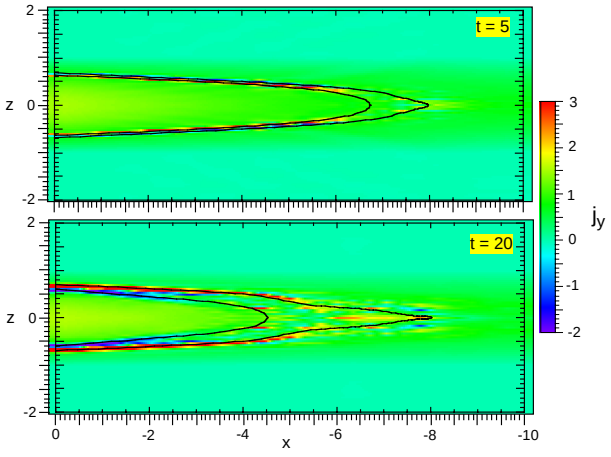

Fig. 7. Current density in the plane y=0 at t=5 and t=20 for the same run as in Fig. 5.

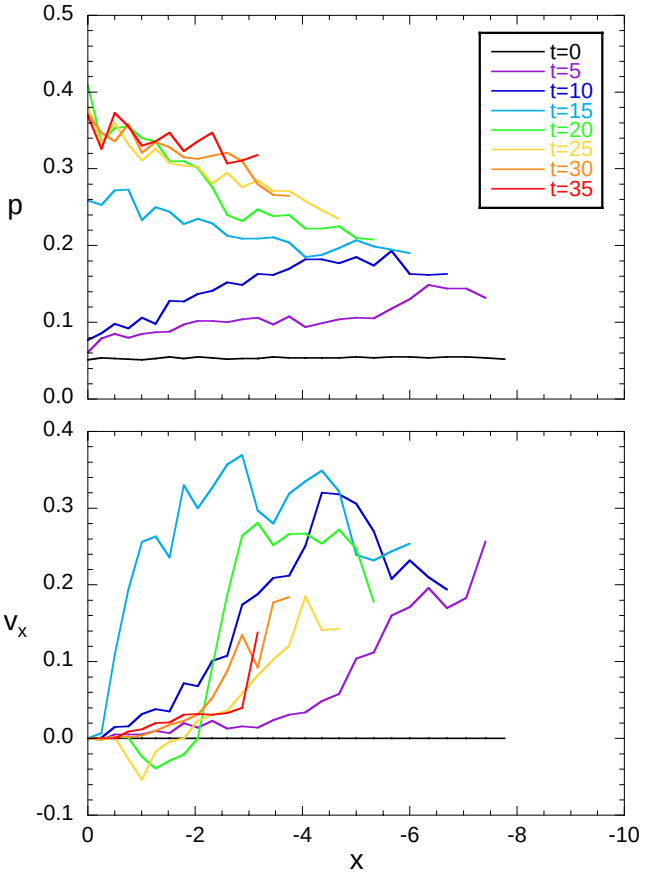

Fig. 8. Evolution of a depleted flux tube with y_m=0.2, showing (from top to bottom) the pressure and the velocity v_x inside the depleted flux tube as functions of x for different times, as indicated by the color coding and the labels given in the top panel.

entropy function $s=p^{1/\gamma}/\rho$, which defines the depleted flux tube. The third panel shows the x component of the velocity, and the fourth panel the magnetic field component B_z, all as functions of x for times t=0, 5, 10, 15, 20 (approximately 0, 2, 4, 6, and 8 min). Figures 5 and 9 demonstrate that the depleted flux tube indeed moves earthward over a significant distance. However, the speed is somewhat smaller than in the simulations of Chen and Wolf (1999), reaching only about 0.3 to 0.4 (equivalent to 300 to 400 km/s). The minimum

of the entropy function s increases somewhat in time, due to numerical diffusion. Nevertheless, the region of reduced entropy, the bubble, remains well defined.

At later times, the tailward end of the bubble is characterized by low-flow speed. As can be seen from the bottom panel of Fig. 9 (and later in Fig. 18), this region assumes roughly the entropy density of the surrounding medium. This is a consequence of numerical dissipation, driven by the small scale of the compressed rear part of the bubble, which is clearly visible at t=15 in Fig. 5.

So far, bubbles were created by reducing the pressure but leaving the density unchanged. This yields a reduced temperature inside the bubble, which is not typical of bursty flows. We therefore also investigated cases where the initial density was also reduced, leaving the temperature unchanged. The earthward propagation of such bubbles is essentially identical to the ones without density reduction and is therefore not shown here. This result supports the view that the bubble propagation is controlled by their entropy content, defined by pV^γ or more generally by the entropy measure Eq. (2), which does not depend on the temperature or density. However, the internal properties are different, as illustrated by Fig. 10, which shows various characteristic quantities in the x, z plane at t=20 for a bubble with y_m=0.2. The top panel shows the change in B_z, subtracting the background field outside the bubble. It clearly shows the dipolarization at the front of the bubble, which is similar to the case without density reduction illustrated in Fig. 9. The subsequent panels of Fig. 10 show the temperature and the density and pressure changes, again subtracting the background fields outside the bubble. They show an increased temperature and decreased density inside the bubble near the equatorial plane. Note, however, that the horns of the bubble show a density increase and an even stronger temperature and pressure increase. This is again due to the compression from the field-aligned flow discussed above.

4.1 Effects of bubble width and depletion

The earthward propagation and the maximum speed of the bubble depend on the width in the y direction. This is demonstrated by Figure 11, which shows the maximum earthward flow speed as a function of time for the three cases with different widths, given by y_m=0.02, 0.2, 2.0. The narrow bubble reaches a maximum speed of ∼0.37 (370 km/s), while the widest bubble reaches only a maximum speed of ∼0.2 (200 km/s), which becomes even smaller at later times.

The maximum speed also depends on the amount of depletion. We used different initial pressure reductions to investigate this problem. Figure 12 shows the maximum earthward speed for bubbles with y_m=0.2 and various amounts of the reduction. The factor f is defined by the reduction $p=p_0+f\cdot p_1$, where p_1 is the unperturbed pressure in the bubble, and p_0 is the uniform background pressure, which is held fixed. Obviously, the more strongly depleted flux tubes achieve higher speed. However, for reasonable values of the

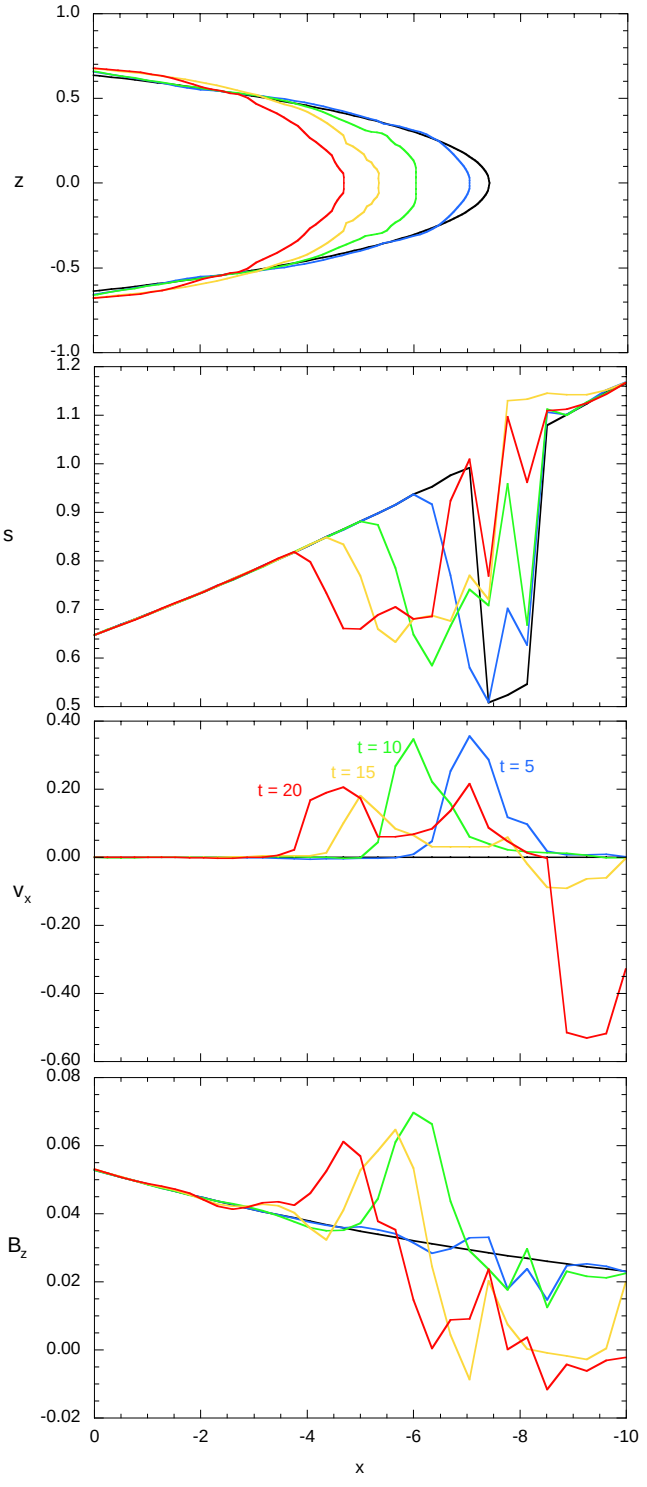

Fig. 9. Evolution of a depleted flux tube with y_m=0.02 along the x-axis, showing (from top to bottom) magnetic field lines at the inner edge of the bubble, the measure of specific entropy $s=p^{1/\gamma}/\rho$, the velocity v_x, and the magnetic field component B_z as functions of x for different times, as indicated by the color coding and the labels given in the third panel.

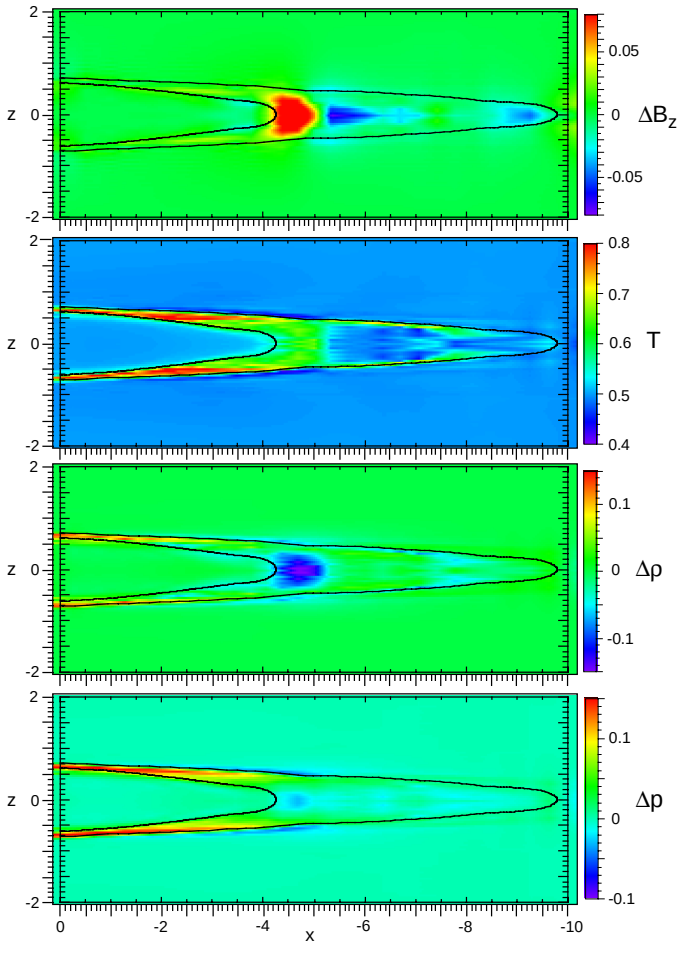

Fig. 10. Properties of a depleted flux tube that also includes an initial density reduction but unchanged temperature, for y_m=0.2 and t=20, showing (from top to bottom) $\Delta B_z = B_z - B_{z,bg}$, where $B_{z,bg}$ is the background field outside the bubble, the temperature, and the change of density $\Delta\rho = \rho - \rho_{bg}$ and pressure $\Delta p = p - p_{bg}$, again subtracting the background fields outside the bubble. The solid lines are magnetic field lines bounding the depleted flux tube. They are identified by tracing the motion of the equatorial crossing points of the initial depleted flux tube.

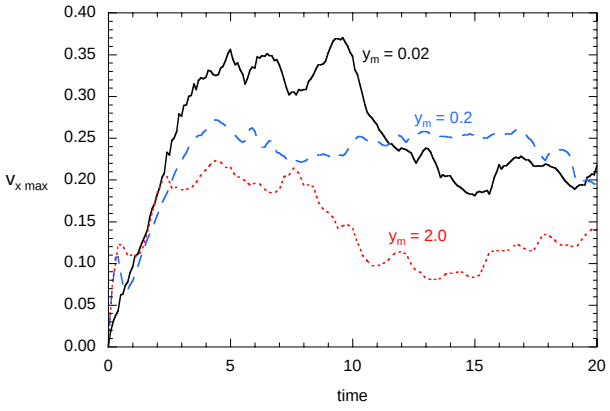

Fig. 11. Maximum earthward flow speed as function of time for bubbles with different widths y_m=0.02 (solid line), y_m=0.2 (dashed line), and y_m=2.0 (dotted line).

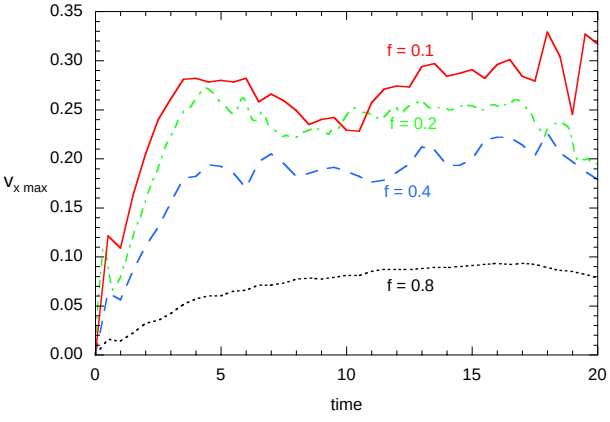

Fig. 12. Maximum earthward flow speed as a function of time for bubbles with y_m=0.2 and different amounts of initial pressure reduction, defined by the factor f (see text).

pressure reduction, the speed still remains moderate, at 0.3 to 0.4 (300 to 400 km/s).

4.2 Effects of initial impulse

In this subsection we investigate the role played by a potential initial acceleration of a bubble, which might result from some process not included in our model, such as localized reconnection. We simply give each plasma element inside the bubble an initial earthward speed, which is proportional to $|x|$ and reaches a maximum of ∼0.4 at the apex of the bubble. The bubble is defined by the reduced entropy function $s = p^{1/\gamma}/\rho$ as before. For comparison, we also investigate cases in which the same initial velocity is given to the same flux tube, but the pressure and entropy are unperturbed. Figure 13 shows the maximum flow speeds as functions of time for the intermediate flux tube (y_m=0.2), for the previous case without initial velocity (black dotted curve), the case with the additional initial velocity (blue solid curve), and the case with initial velocity but no pressure perturbation (red dash-dotted curve). The two cases with the depletion of the flux tube differ initially; however, they approach approximately the same speed after approximately t=5. In contrast, the flux tube that is not depleted is essentially stopped after about 10 Alfvén times. This is further demonstrated by Fig. 14, which shows the velocity profiles $v_x(x)$ for the three cases for various times indicated by color. This figure shows more clearly that the undepleted but accelerated flux tube does not propagate significantly towards Earth.

4.3 Anisotropy

In this subsection we investigate the possible effects of a pressure anisotropy, using the double-adiabatic approximation, in which the pressure tensor $\underline{\mathbf{P}}$ is gyrotropic, defined by

$$\underline{\mathbf{P}} = p_\perp \underline{\mathbf{I}} + (p_\parallel - p_\perp)\mathbf{bb}, \quad (8)$$

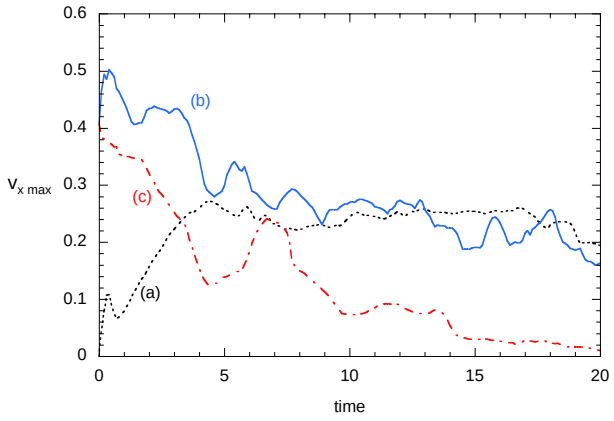

Fig. 13. Maximum earthward flow speed as a function of time for bubbles with y_m=0.2 and **(a)** pressure reduction but no initial velocity (dotted line), **(b)** pressure reduction and initial velocity (solid line), **(c)** no pressure reduction but finite initial velocity (dash-dotted line).

where $\underline{\mathbf{I}}$ is the unit tensor and $\mathbf{b}=\mathbf{B}/B$ the unit vector in the direction of the magnetic field. In the absence of heat conduction, and not regarding the coupling of the pressure components by microinstabilities, the equations for the parallel and perpendicular components of the pressure tensor can then be written as (Hesse and Birn, 1992)

$$\frac{\partial p_\parallel}{\partial t} = -\nabla\cdot(p_\parallel \mathbf{v}) - 2p_\parallel \mathbf{b}\cdot(\nabla\mathbf{v})\cdot\mathbf{b} \qquad (9)$$

$$\frac{\partial p_\perp}{\partial t} = -\nabla\cdot(p_\perp \mathbf{v}) - p_\perp[\nabla\cdot\mathbf{v} - \mathbf{b}\cdot(\nabla\mathbf{v})\cdot\mathbf{b}] \qquad (10)$$

with the modified momentum equation

$$\frac{\partial \rho\mathbf{v}}{\partial t} = -\nabla\cdot(\rho\mathbf{v}\mathbf{v}) - \nabla\left(p+\frac{B^2}{2}\right) + \nabla\cdot\left[\left(1-\frac{p_\parallel - p_\perp}{B^2}\right)\mathbf{B}\mathbf{B}\right]. \qquad (11)$$

Equations (9) and (10) replace the standard adiabatic pressure equation and can be shown to be equivalent to the conservation of the two invariants $p_\perp/\rho B$ and $p_\parallel B^2/\rho^3$ of double-adiabatic magnetofluid theory. The modified double-adiabatic MHD equations are again solved by our explicit leapfrog scheme, using the Dufort-Frankel approximation to replace the pressure factors in Eqs. (9) and (10) by the time-centered average of the values at the new and the previous time step.

The initial perturbation is identical to the case shown in the bottom panel of Fig. 1, reducing both $p_\perp$ and $p_\parallel$ in a narrow flux tube with y_m=0.02. Figure 15 demonstrates the early evolution after the initial pressure reduction, showing $p_\perp$ and $p_\parallel$ as functions of z at x=−7.4, y=0. The perpendicular pressure component recovers very rapidly to its unperturbed value. This is not unexpected, because in a stretched tail-like equilibrium governed by a gyroptropic pressure, the balance of $p_\perp+B^2/2$ replaces the balance of the total pressure $p+B^2/2$ (Nötzel et al., 1985). It is somewhat less expected that, after about 1–2 Alfvén times, the parallel pressure component also returns to its unperturbed value, so that the pressure again becomes nearly isotropic.

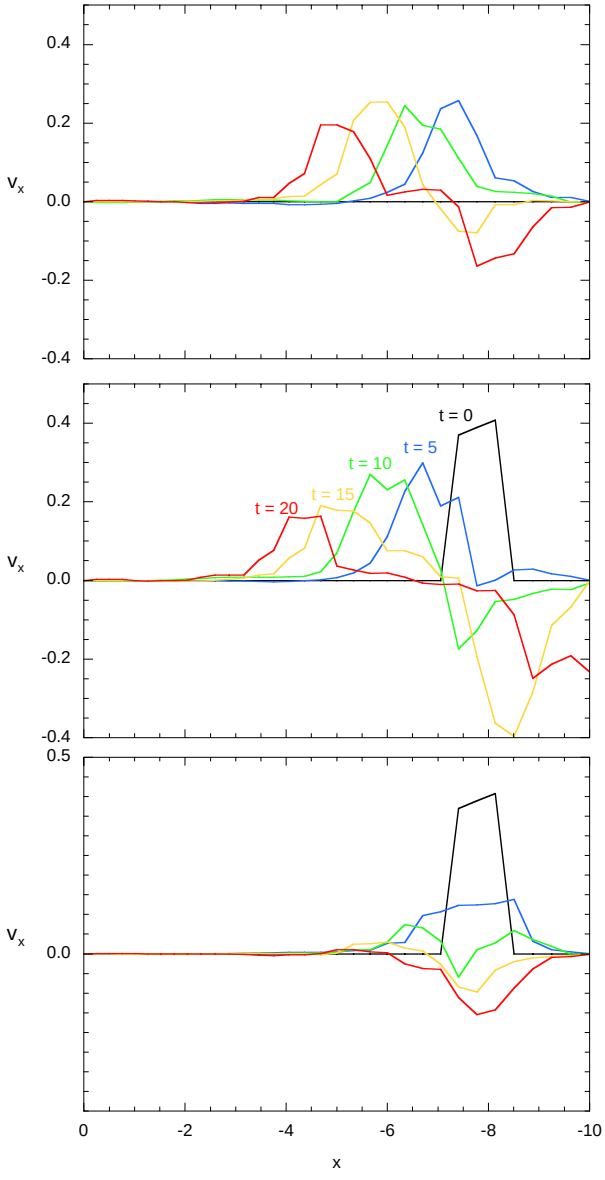

Fig. 14. Velocity profiles $v_x(x)$ at various times for the three cases of Fig. 13, **(a)** pressure reduction but no initial velocity, **(b)** pressure reduction and initial velocity, **(c)** no pressure reduction but finite initial velocity.

Perhaps as a consequence of this near isotropy, the subsequent motion is not much different from the isotropic case. This is demonstrated by Fig. 16, which shows, for a bubble with y_m=0.2, the maximum earthward speed as a function of time for the anisotropic case (solid line) in comparison to the isotropic case (dotted line). The anisotropic case shows more fluctuations, but the overall speed is similar. (The large fluctuations eventually lead to numerical instability, so that the anisotropic case could not be integrated further.)

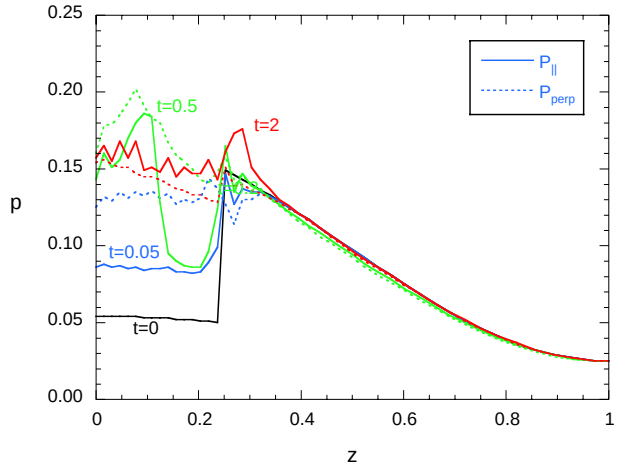

Fig. 15. Plasma pressure components for a narrow flux tube with y_m=0.02 in a double-adiabatic model, at x=−7.4, y=0 as a function of z at different times, as indicated.

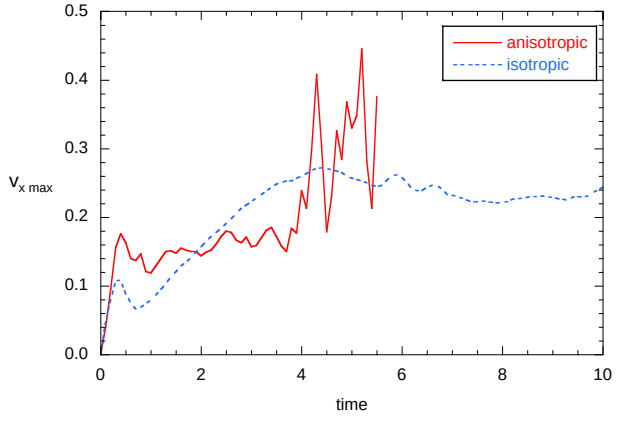

Fig. 16. Maximum earthward flow speed as a function of time for a bubble with y_m=0.2 governed by a double-adiabatic anisotropic model (solid line), compared to the isotropic model (dotted line).

4.4 Field-aligned currents

In this section we investigate the relationship between the depleted flux tube and the generation of field-aligned currents. Chen and Wolf (1993) suggested that an earthward moving bubble should cause field-aligned currents of the same type as the substorm current wedge, that is, earthward on the dawnside and tailward on the duskside. Nakamura et al. (2001) found a good correlation between earthward flow bursts and auroral activations, which mapped to their duskward edge, consistent with the coupling through tailward currrents. Figure 17 demonstrates that indeed such field-aligned currents are present along the outer edges of the bubble flux tube and extend toward the Earth. Figure 17 shows the color-coded magnitude of the x component of the field-aligned current density $\mathbf{j}_\parallel$ near the inner (earthward) boundary for the three different bubble widths at t=20.

The density of these field-aligned currents is very similar for the three cases, however, the integrated magnitude varies from less than 10^4 A for the narrow bubble to a few times 10^5 A for the widest bubble.

Figure 18 illustrates that the diversion of perpendicular to field-aligned currents occurs along the outer edges in y of the bubble in the equatorial plane at t=15. The top panel shows the entropy function $s=p^{1/\gamma}/\rho$, which identifies the bubble, while the bottom panel shows the x component of the flow speed, again demonstrating that the earthward motion is confined to the bubble. The center panel shows the diversion of the parallel current density ($\nabla\cdot\mathbf{j}_\parallel$), integrated over z. In each panel velocity vectors with $v>0.05$ have been overlaid. The black contours in each panel show the outline of the initial bubble (rectangle) and its deformation at t=15. It is obvious that the earthward flow creates vortices on its flanks, which wind up the magnetic field lines and thereby generate field-aligned currents, which are diverted from the cross-tail current. The top panel shows that the initial reduced entropy in these wound-up parts of the bubble is not conserved, and the entropy density of the surrounding medium is assumed. This is due to numerical diffusion in the simulation. However, a similar effect might be expected from physical dissipation associated with the small scales in these distorted regions.

The main part of the bubble is characterized by an earthward flow of 200–300 km/s. It has widened through the vortical motion discussed above. It extends tailward into a very narrow tail with much lower speed, which has been compressed by converging motion in y. As a consequence, the earthward speed is largest at y=0. This is the reason why the very end has assumed a fork shape. The narrow extent in y, together with a narrow extent in z (Fig. 5), is also the reason why the entropy reduction has become numerically dissipated, so that this part has assumed the entropy density of the surrounding medium.

Figure 19 further illustrates the mechanism of field-aligned current generation, together with the mechanism for enhancing the pressure in the horns of the bubble (top panel). When the bubble moves earthward, field lines that are located more earthward become pushed outward, out of the way of the bubble. This leads to a vortex flow outside the bubble, causing a twist or shear in the magnetic field, which corresponds to the presence of field-aligned currents. The vortex flows also correspond to electric fields, which have a positive divergence on the dawn side and negative divergence on the dusk side, corresponding to positive and negative space charges, respectively. We emphasize, however, that these space charges are not the generation mechanism for the field-aligned currents, because their effect is negligible, due to the quasi-neutrality approximation.

5 Conclusions

Using fully three-dimensional MHD simulations, we have investigated the dynamics of magnetotail flux tubes that have reduced entropy content (bubbles). Three different widths

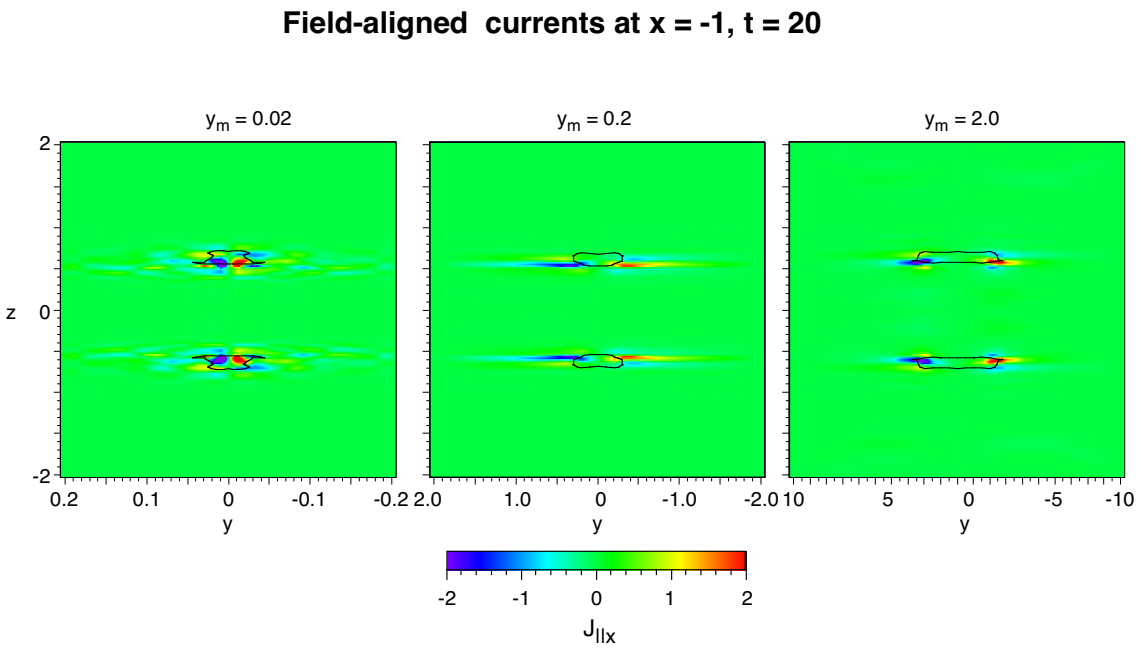

Fig. 17. Field-aligned current densities $\mathbf{j}_{\parallel x}$ at $x=-1$ near the inner (earthward) boundary at $t=20$ for three different bubble widths. The black contours outline the bubble flux tubes.

of the depleted flux tubes were considered, corresponding to ∼1000 km, ∼1.6 R_E, and ∼16 R_E total width, based on a scale length of 4 R_E for the plasma/current sheet half-width. Our simulations addressed fundamental properties of the propagation and dynamics of such flux tubes rather than the actual formation process. In fact, some of the assumptions, in particular the assumption that the flux tube pressure is initially reduced uniformly, are rather questionable in view of the fact that the evolution leads to nonuniform pressure along the flux tube. Nevertheless, the simulations provide insight into the processes that enable the propagation of flux tubes from the more distant tail towards the Earth.

Our scope was similar to that of Chen and Wolf (1999), however, our approach differed in several important aspects. First, we used a fully three-dimensional MHD code. Second, we also fully investigated the initial phase after the depletion, which was bypassed by Chen and Wolf by assuming that pressure equilibrium in y and z was re-established, while the pressure remained constant along the depleted field line. Our results demonstrated that restoring the pressure balance in y and z indeed takes only a very short time, a fraction of an Alfvén time to about 1 Alfvén time (that is, a few to tens of seconds for typical tail parameters). Restoring the pressure balance along the field lines, however, takes much longer, and competes with the dynamics and motion of the bubble. Thus, the pressure balance along the field line was not maintained during the simulations.

The earthward transport of the depleted flux tube, combined with the initial pressure imbalance along the flux tube, leads to significant field-aligned earthward flow, which leads to a compression and heating of the near-Earth parts (horns). As a consequence, the initial pressure and temperature reduction becomes reversed in these horns of the depleted flux tube. This pressure increase, as well as the earthward flow, could be the cause of enhanced proton and electron precipitation observed recently by Sergeev et al. (2004), as a characteristic of auroral streamers, which are presumably associated with plasma sheet bubbles, in the equatorward portion of the auroral oval.

The pressure increase in the horns of the bubble leads to a decrease of the magnetic field strength, from pressure balance with the surrounding field, whereas the near-equatorial signature remains a magnetic field enhancement. The localized magnetic field reduction in the horns of the bubble is associated with a current perturbation, consisting of thin current layers of a dawnward direction below the depleted flux tube and enhanced duskward current above, closing around the flux tube through northward and southward currents. Although in the present model these effects are associated with a solid, impenetrable near-Earth boundary, similar effects are to be expected from the mirroring of particles approaching the Earth.

We should add a comment on the definition of the bubble under the described conditions when the pressure becomes enhanced in part of the flux tube. Although one might expect that this changes the bubble to a “blob”, defined by enhanced entropy content, this is not the case; the entropy density, as measured by $p^{1/\gamma}/\rho$, remains reduced. Furthermore, the global entropy defined by Eq. (2) also remains reduced on the depleted flux tube during its evolution and transport.

Despite the differences in the early evolution, our results are qualitatively similar to those of Chen and Wolf (1999). The reduction of the entropy content of a flux tube is crucial in enabling its earthward propagation and its eventual

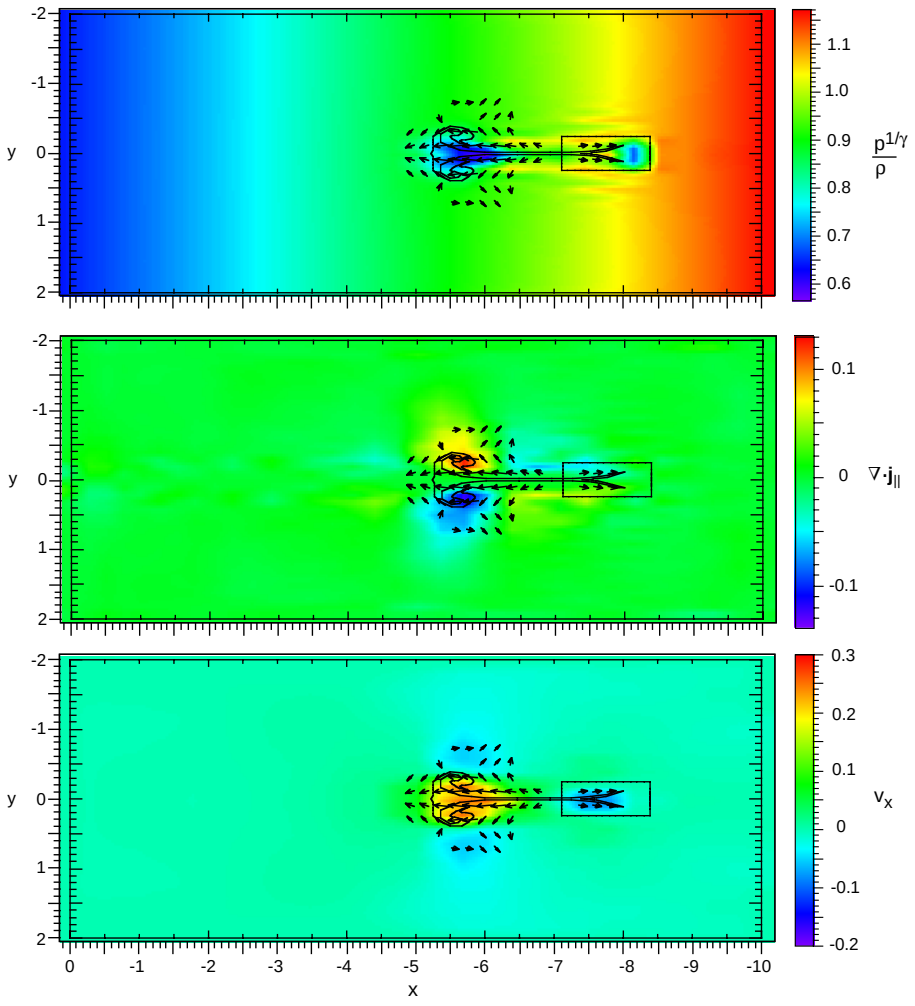

Fig. 18. Bubble properties in the equatorial plane at t=15 for a depleted flux tube with y_m=0.2. The top panel shows the entropy function $s=p^{1/\gamma}/\rho$, the center panel the diversion of the parallel current density ($\nabla\cdot\mathbf{j}_\parallel$), integrated over z, and the bottom panel shows the x component of the flow speed. Black arrows represent velocity vectors with $v>0.05$, and the black contours outline the initial bubble boundary (rectangle) and its deformation at t=15.

penetration into the near tail. A simple initial acceleration without the entropy reduction is not sufficient and does not allow for significant earthward progation. However, the speeds attained in our simulation, were only of the order of 200–400 km/s, smaller than those found by Chen and Wolf and only marginally in the range associated with bursty bulk flows. It hence seems that both the entropy reduction and the plasma acceleration play an important role in the generation of fast plasma flows and their propagation into the near tail.

Our model is not directly a model of bursty bulk flows in the plasma sheet (Baumjohann et al., 1990; Angelopoulos et al., 1992). In fact, some of the features that are a direct consequence of our initial perturbation appear to be inconsistent with typical BBF observations in the near tail, specifically the fact that by construction, for most of our models, the density in our bubbles is initially unchanged and becomes even enhanced from the early compression, while the temperature is reduced. However, this effect is reversed at later times in the higher-latitude portions of the flux tube closer to Earth. Also, models that include an initial density reduction as well, show virtually unchanged earthward propagation. Thus, our models appear consistent with plasma-depleted flux tubes detected in the midtail by Sergeev et al. (1996b). We note that simulations of magnetic reconnection in the near-tail lead to more realistic properties, showing a temperature increase and density decrease in the region of earthward flows (Birn et al., 1996b). Basic differences can be attributed to the fact that reconnection leads to a reduction of the flux tube volume rather than the pressure and that the plasma acceleration not only occurs at the reconnection site but also along slow shocks extending from that site.

Several effects were found to influence the propagation speed, primarily the amount of the initial pressure or entropy reduction, and the width of the depleted bubble in the cross-tail direction. Stronger entropy reduction leads to faster speeds, and wider bubbles tend to be slower than narrow ones, for the same entropy reduction. Pressure anisotropies, explored in a double-adiabatic fluid model, lead only to

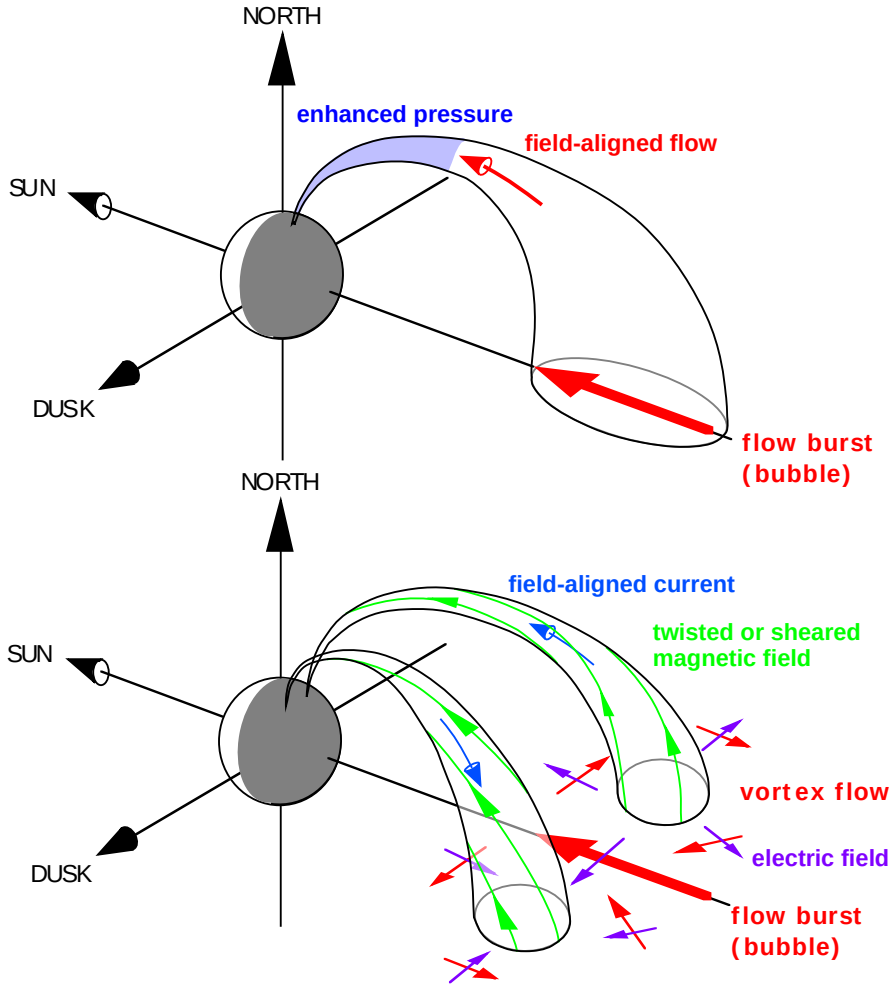

Fig. 19. Schematic illustrating the mechanisms of pressure enhancement from the slow-down of field-aligned flow near the Earth (top) and field-aligned current generation (bottom). When the bubble moves earthward, field lines that are located more earthward become pushed outward, out of the way of the bubble. This leads to a vortex flow outside the bubble, causing a twist or shear in the magnetic field, which corresponds to the presence of field-aligned currents of region-1 sense.

insignificant changes in the propagation speed. Recently, Ji and Wolf (2003) also investigated the propagation of a thin filament with reduced pressure within double-adiabatic MHD theory. They also found that the filament moves earthward at roughly the same velocity as in the isotropic case, but the pressure became very anisotropic as the filament shortened, which had significant effects on wave propagation and eventually stability.

Earthward moving bubbles were found to be associated with field-aligned current systems, directed earthward on the dawnward edge and tailward on the duskward edge. This is consistent with current systems attributed to observed bursty bulk flows, relevant for their connection with auroral features (Sergeev et al., 1996a; Kauristie et al., 2000; Nakamura et al., 2001; Sergeev et al., 2004). In the MHD model, the field-aligned currents are generated by the twist of magnetic flux tubes through vortical plasma motion outside the bubble near its earthward front. This may be visualized as a bubble plowing its way through surrounding field lines and pushing them to the side, while becoming more dipolar itself.

Acknowledgements. This work was supported by the U. S. Department of Energy's Office of Basic Energy Sciences through its Geosciences Research Program, by NASA's Sun Earth Connection Theory Program, and by the National Science Foundation through grant ATM-0202306. Research at UCLA was supported by grant ATM 00-97143 from the National Science Foundation and by Los Alamos National Laboratory IGPP grant #02-1212.

Topical Editor T. Pulkkinen thanks H. Spence and another referee for their help in evaluating this paper.

References

Angelopoulos, V., Baumjohann, W., Kennel, C. F., Coroniti, F. V., Kivelson, M. G., Pellat, R., Walker, R. J., Lühr, H., and Paschmann, G.: Bursty bulk flows in the inner central plasma sheet, J. Geophys. Res., 97, 4027, 1992.

Baumjohann, W., Paschmann, G., and Lühr, H.: Characteristics of high-speed ion flows in the plasma sheet, J. Geophys. Res., 95, 3801, 1990.

Birn, J., Iinoya, F., Brackbill, J., and Hesse, M.: A comparison of MHD simulations of magnetotail dynamics, Geophys. Res. Lett.,

23, 323, 1996a.
Birn, J., Hesse, M., and Schindler, K.: MHD simulations of magnetotail dynamics, J. Geophys. Res., 101, 12 939, 1996b.
Chen, C. X. and Wolf, R. A.: Interpretation of high-speed flows in the plasma sheet, J. Geophys. Res., 98, 21 409, 1993.
Chen, C. X. and Wolf, R. A.: Theory of thin-filament motion in Earth's magnetotail and its application to bursty bulk flows, J. Geophys. Res., 104, 14 613, 1999.
Erickson, G. M. and Wolf, R. A.: Is steady convection possible in Earth's magnetotail, Geophys. Res. Lett., 7, 897, 1980.
Goertz, C. K. and Baumjohann, W.: On the thermodynamics of the plasma sheet, J. Geophys. Res., 96, 20 991, 1991.
Hesse, M. and Birn, J.: MHD modeling of magnetotail instability with anisotropic pressure, J. Geophys. Res., 97, 10 643, 1992.
Ji, S. and Wolf, R. A.: Double-adiabatic-MHD theory for motion of a thin magnetic filament and possible implications for bursty bulk flows, J. Geophys. Res., 108, (A5), 1191, doi:10.1029/2002JA009655, 2003.
Kauristie, K., Sergeev, V. A., Kubyshkina, M. V., Pulkkinen, T. I., Angelopoulos, V., Phan, T., Lin, R. P., and Slavin, J. A.: A conjugate study of wind and ground-based observations during transient plasma sheet flows, J. Geophys. Res., 105, 10 677, 2000.
Kivelson, M. G. and Spence, H. E.: On the possibility of quasi-static convection in the quiet magnetotail, Geophys. Res. Lett., 15, 1541, 1988.
Nakamura, R., Baumjohann, W., Schödel, R., Brittnacher, M., Sergeev, V. A., Kubyshkina, M., Mukai, T., and Liou, K.: Earthward flow bursts, auroral streamers, and small expansions, J. Geophys. Res., 106, 10 791, 2001.
Nötzel, A., Schindler, K., and Birn, J.: On the cause of approximate pressure isotropy in the quiet near-Earth plasma sheet, J. Geophys. Res., 85, 8293, 1985.
Pontius Jr., D. H. and Wolf, R. A.: Transient flux tubes in the terrestrial magnetosphere, Geophys. Res. Lett., 17, 49, 1990.
Schindler, K. and Birn, J.: Self-consistent theory of time-dependent convection in the magnetotail, J. Geophys. Res., 87, 2263, 1982.
Sergeev, V., Pellinen, R., and Pulkkinen, T.: Steady magnetospheric convection: A review of recent results, Space Sci. Rev., 551, 1996a.
Sergeev, V. A., Angelopoulos, V., Gosling, J. T., Cattell, C. A., and Russell, C. T.: Detection of localized, plasma-depleted flux tubes or bubbles in the midtail plasma sheet, J. Geophys. Res., 101, 10 817, 1996b.
Sergeev, V., Liou, K., Newell, P. T., Ohtani, S.-I., Hairsto, M. R., and Rich, F.: Auroral streamers: Characteristics of associated precipitation, convection and field-aligned currents, J. Geophys. Res., 101, 10 817, 1996b.
Sergeev, V. A., Liou, K., Newell, P. T., Ohtani, S.-I., Hairston, M. R., and Rich, F.: Auroral streamers: Characteristics of associated precipitation, convection and field-aligned currents, Ann. Geophys., 22, 2, 537–548, 2004.
Voigt, G.-H.: Magnetospheric equilibrium configurations and slow adiabatic convection, Solar Wind-Magnetosphere Coupling, Terra Science, Tokyo, 263, 1986.